BIOMEDICAL ENGINEERING

Carnegie Mellon University

# 2012 Summer Undergraduate Research Program (SURP) Research Poster Presentations

**August 1, 2012**

**University Center, Connan Room**

**Noon to 2:00 PM**

**Conformation and binding partner characterization of nucleoskeletal proteins**

Matt Biegler, Kelli Coffey, Kris Dahl. Carnegie Mellon University.

**Introduction:**

The nucleoskeleton inside of cells helps regulate gene expression and protect the genome from mechanical stresses. Little is known about the proteins that make up the nucleoskeleton including the lamins, lamin A and lamin B, which form independent intermediate filament networks and the spring like protein, alphaII-spectrin. Deviations in these wild-type nucleoskeletal proteins are responsible for many disorders, such as Hutchinson-Gilford Progeria Syndrome (HGPS) and Emery-Dreifuss Muscular Dystrophy. The Lamin B1 tail, a permanently lipidated and intrinsically disordered peptide, shares many characteristics with the HGPS Lamin A mutant, Δ50. Determining the similarity relationship of function between these proteins would fill existing gaps in molecular biology and nuclear pathology research.

**Materials and Methods:**

Protein DNA for the Lamin B1 tail was procured from collaborating labs and validated for subcloning. The DNA is cut using restriction enzymes, XhoI and BamHI, and separated by gel electrophoresis. The cut insert is then ligated into a ||GST1 vector used for Glutathione bead purification. DNA sequencing was used to verify the sequence for expression. The subcloned plasmid is transformed into BL21-RIPL strain E.coli and used to express the protein. Following purification of the expression process, the protein is lipidated and tested in various salt solutions by tryptophan fluorescence to observe structural conformation and aggregation states. This data is used to compare with data collected from other lamin and nucleoskeletal proteins studied previously by the Dahl Lab.

**Results and Discussion:**

Currently, the Lamin B1 tail DNA insert has been subcloned into the ||GST1 vector (Figure 1) and confirmed using sequencing data provided by Genemed Synthesis, Inc. in San Antonio, Texas. Sequencing has determined the insert to be ordered correctly and in the proper reference frame for translation into protein. However, protein expressions in BL21-RIPL strain E. coli have, so far, proven difficult. Further work resolving potential obstacles in the plasmid or other aspects of the expression process is required.

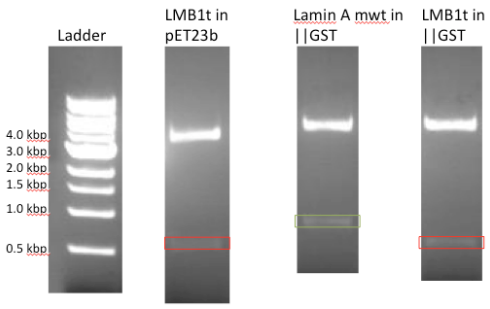


**Figure 1. Size determination of DNA plasmids and inserts used in subcloning procedure. Insert of Lamin A mwt in ||GST1 was removed and replaced with the Lamin B1 tail insert from the pET23b plasmid procured from the Wilson Lab at Johns Hopkins University.**

**Conclusions:** Further results and conclusions relating to the Lamin B1 tail are pending success of the protein expresssion and purification process.

**Acknowledgements:** I would like to thank Dr. Kris Dahl, PhD, Agnieszka Kalinowski, PhD, Kelli Coffey, and the rest of the Dahl Lab. I also acknowledge the Department of Biomedical Engineering for this opportunity, as well as The Progeria Research Foundation and the National Institutes of Health for funding of our research.

**Ferrihydrite (Fh): Structural Models and Biological Significance**

Tomas J. Dardet,[¥,Γ] Priyanka Anand,[¥] Michael E. McHenry[¥]
[¥]Department of Materials Science & Engineering, Carnegie Mellon University, Pittsburgh, Pennsylvania, 15213, U.S.A.
[Γ]Department of Biomedical Engineering, Carnegie Mellon University, Pittsburgh, Pennsylvania, 15213, U.S.A

**Introduction:** Ferrihydrite (Fh) is a Nano crystalline hydrous Fe (III) Oxy-hydroxide with variable crystallinity and composition. It is generally classified by the number of powder X-Ray Diffraction (XRD) peaks the material exhibits, ranging from 2 to 6 broad Bragg peaks. These are termed 2-line and 6-line Fh respectively and the degree of crystallinity of Fh increases from 2 to 6-line progressively. The nanocrystalline, highly defective, and variable water content of this mineral has resulted in many competing structural models to arise, the main two of which are Michel et al.'s single phase model which contains tetrahedral and octahedrally coordinated Fe(III) and Drits et al.'s three phase model containing a defective and defect free refinement with ultradispersed hematite and only octahedrally coordinated Fe(III). Criticisms for both models are abundant and as such a new structural model must be developed. Knowledge of the Fh structural model is biologically significant due to the fact that Fh, mixed with phosphate, magnetite and hematite, has been found to be the main fraction of the inorganic core of Ferritin, the iron storage protein in various biological systems. Iron accumulation and phase transformation in the brain has been linked to Alzheimer 's disease as well as other neurodegenerative disorders, and knowledge of the Fh structure would allow accurate computational modeling. The goal of this work is to review the literature, understand the various synthetic pathways of the Iron Oxy(Hydrox)-ides by modifying synthetic procedures and explore and develop new techniques to both determine a structural model that agrees with recent findings and explore the magnetic and conductive properties of different phase fractions in the Ferritin protein.

**Materials and Methods:** All of the reagents utilized were bought from Sigma-Aldrich and are of analytical grade (99%). Both 2 and 6-line Fh were synthesized through forced hydrolysis of $Fe(NO_3)_3 \cdot 9H_2O$. 2-line Fh was synthesized utilizing the synthesis procedure detailed in Li Z. et al. Two distinct synthesis procedures for 6-line Fh have been attempted. With Mohapatra et al.'s procedure we attempt to produce nano-rod shaped 6-line Fh particles of 7-20 nm width and 50-200 nm length. With Carta et al.'s procedure we attempt to produce spherical 6-line Fh particles with a mean diameter of 3 nm. Characterization of the Fh nanoparticles was done with XRD supplemented by color comparison.

**Results and Discussion:** XRD with Cu-Kα monochromatic radiation of the 2-line Fh sample reproduced its characteristic two broad peaks at approximately 33° and 61.5° 2θ angle, representing the (110) and (300) planes respectively. The XRD pattern in addition to the dark reddish-brown color of our synthesized powder gives preliminary evidence of 2-line ferrihydrite. However, XRD patterns for the nano-rod and spherical 6-line Fh synthesis procedures failed to reproduce the characteristic 6 broad peak pattern. The nano-rod procedure resulted in an XRD pattern characteristic of hematite ($\alpha$-$Fe_2O_3$). The formation of hematite hints at a much too rapid hydrolysis rate and after reviewing the parameters utilized a new sample shall be prepared with a lower hydrolysis rate. The spherical 6-line procedure resulted in an unrecognizable XRD pattern.

**Conclusions:** Preliminary results suggest that 2-line Fh synthesis has succeeded in order to proceed with structural and magnetic characterization. Additionally attempts at synthesizing 6-line Fh have yielded a potential simple hematite synthesis procedure and troubleshooting to produce the nano-rods seems promising. In order to study the effects of agglomeration on the transformation of 2 and 6 line Fh to more stable phases future work consists of trapping the nanoparticles in a glass or polymer and performing XRD scans at varying temperatures and pressures to induce potential crystallization independent of agglomeration.

**PROTOCOL DEVELOPMENT FOR TESTING CALCIUM ALUMINATE AS A BONE SUBSTITUTE**

Kartik Goyal, Mark Miller, Pat Schimoler. Allegheny General Hospital Orthopaedic Biomechanics Research Laboratory.

**Introduction:** Bone serves three major functions in the human body. The first function is to provide structure to the body. The second is to protect the major organs, muscles and tissues. The third general function is bone possesses marrow which is very important for the body's immune system. When there is serious injury or damage to one's bone, a common procedure to treat this is bone grafting. Basically bone grafting takes bone from somewhere else in the patient's body, called an autograft, or from a generous donor, known as an allograft. Bone grafting is an increasingly common surgery performed in the United States. Unfortunately, while the demand for bone grafting is ever increasing, the amount of donors is insufficient to meet this demand. To meet the needs of the growing number of patients, bone substitutes are needed. Bone substitutes are materials used to artificially replace missing bone. Bone substitutes need to have similar structural properties as bone and allow surrounding bone tissue to grow into the substitute for a natural integration via porosity and growth proteins. Bone substitutes can simplify the grafting process by eliminating the need for donors and facilitate the healing process. In this research, calcium aluminate is investigated for its viability as a bone substitute material.

**Materials and Methods:** To make the samples for testing, the cement is created using typically one pound of calcium aluminate mix which is mixed with water at a 0.22 water-to-mix ratio. The cement is shaken periodically to release trapped air pockets. The mixture is then inserted into molds for beams with dimensions 1" x 7" x .665" and cylinders .807" in diameter, which can be drilled to make annuli with inner diameter .25" and outer diameter .807", depending on the test to be conducted. After curing for 24 hours, the samples are then mounted onto the MTS Bionix 858 Test System to conduct tests in compression and four point bending. Displacements in the samples can be measured by placing markers on the surface of the sample and tracking them using a Spicatek camera system.

**Results and Discussion:** Using data from both the MTS system and the Spicatek marker tracking, the following material properties can be calculated for the calcium aluminate, which is compared to bone:

| Property | Calcium Aluminate | Bone |
|---|---|---|
| Bending Stress | 9.6 MPa | 25 to 315 MPa |
| Compressive Stress | 24.1 MPa | 70 to 280 MPa |
| Bending Modulus | 8680 MPa | Expected for Calcium Aluminate: 8000 MPa to 12000 MPa |
| Young's Modulus | 9200 MPa | 5000-21000 MPa |

The initial estimation for the maximum compressive stress was 40 MPa, however a cylinder created based on this assumption was unable to be compressed by the MTS system, meaning 40 MPa was too low. However, an annulus was able to be yield at 24.1 MPa, which would suggest that drilling a hole into the sample causes damage to the cylinder and has an effect on the results.

**Conclusions:** The tabulated results suggest that calcium aluminate is reasonably weaker than bone. According to previous literature, this is not the case. In this experiment only one beam was tested along with two cylinders. Therefore, more samples need to be tested to determine consistency of the results. A new way to create an annulus must be developed to provide accurate results. Also, varying porosities can be investigated for optimized bone in-growth and stiffness.

**Acknowledgements:** The author would like to thank the members of the Orthopaedic Biomechanics Research Laboratory of the Allegheny General Hospital for their support with this project. Thanks also go to the Biomedical Engineering department at Carnegie Mellon University for providing this opportunity to do research.

**In Vitro Microvascular Sonothrombolysis**

Allen Kim,
UPMC Center for Ultrasound Molecular Imaging and Therapeutics, Carnegie Mellon University Biomedical Engineering

**Introduction:** Coronary artery disease and stroke are currently two leading causes of disability and death in the United States. A commonly used technique to treat acute coronary syndromes is percutaneous interventions (PCI), but is not without limitations. Even after the occluded artery has been recanalized, up to 40% of patients suffer from a lack of microvascular perfusion ('no-reflow') due to embolization of microthrombi and plaque complexes downstream from the treated lesion. 'No-reflow' is associated with increased risk of malignant arrhythmias, reduced ejection fraction, and development of congestive heart failure and cardiac death. At our lab a new treatment is being developed to overcome 'no-reflow', utilizing ultrasound and microbubbles. Currently, sonothrombolysis (lysis of emboli using ultrasound and microbubbles) is studied mainly using an *in vitro* setup. However, the current setup has some limitations, such as limited reproducibility due to difficulty with alignment of the phantom and the transducer. The goal of this project was to develop a new *in vitro* setup to overcome described problems.

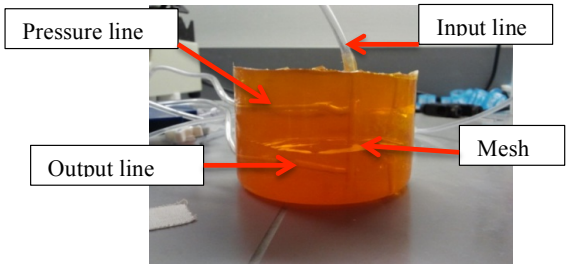


**Figure 1.** The rubber phantom used in the experiments with important components labeled.

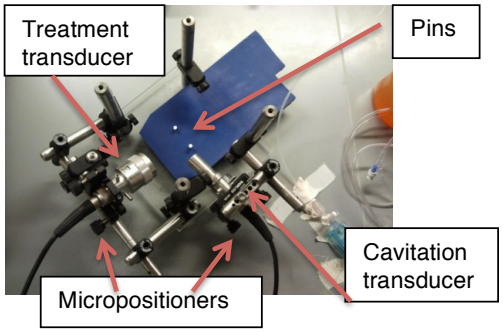


**Figure 2.** The transducer and rubber phantom holder that was used for the experiment. The phantom is placed on the pins.

**Materials and Method:** The in vitro setup can be broken down into two components, the rubber phantom and the apparatus holding the ultrasound transducers. *Rubber phantom* The rubber phantom was created by melting M-F Hardener and Softener at a ratio (400:3) to obtain the desired stiffness. Acoustic attenuation was tested on samples of different stiffness's but no differences were found, but stiffness is of importance because the phantom needed to maintain a certain level of rigidity as not to alter alignment. A 4mm diameter channel was molded into the phantom to mimic the artery. A perpendicular cut slightly below the middle of the channel is made to insert a mesh where the clot will be placed (see figure 1). *Apparatus* The transducer apparatus consists of stainless steel optical posts and components that rigidly hold the ultrasound transducers aimed at a mesh inside the rubber phantom (see figure 2). A new transducer micropositioning system was utilized to give the transducers two axis of rotational motion. The setup was designed using Autodesk Inventor CAD software before being assembled. Alignment of the phantom and transducer was achieved by using a pin system that insures that the rubber phantom is placed in the exact same spot every time it was inserted into the holder. In addition, the micropositioning system enabled small adjustments if either transducer was off target.

**Results:** The setup was tested by repeating a sonothrombolysis experiment (N=3) using the constant parameters of 1.5MPa of acoustic strength, a microbubble concentration of 2e5 per mL, Lipid/Polymer microbubbles and 1000 and 5000 cycles of ultrasound bursts. Similar trends were found in both the lipid and polymer microbubbles. In both the lipid and polymer, the 5000 cycle experiments had a higher initial rate of pressure decline compared to the 1000 cycle experiments. These trends, along with easier preparation procedures can give us confidence in this setup's reproducibility.

**Conclusions:** The new *in vitro* setup improved the alignment of the rubber phantom with the transducer resulting in reproducible data.

## *DROSOPHILA MELANOGASTER* AS A MODEL IN THE STUDY OF NEURODEGENERATIVE DISEASES

Rebecca Lui[1,2], [1]Department of Chemical Engineering; [2]Department of Biomedical Engineering
Carnegie Mellon University, Pittsburgh, Pennsylvania

**Introduction:** *Drosophila melanogaster*, also known as the common fruit fly, is often used as a model system in many physiological, genetic, developmental, and disease studies. The fruit fly has many advantages as a biological model, including low cost, a short and rapid life cycle, physiological and genetic tractability, the large amount of resources already available for studies, and convenience in inducing mutations. One useful application of the *Drosophila* model is in the study of neurodegenerative diseases, such as Alzheimer's disease and Parkinson's disease. Axonal transport, which is sometimes abnormal in neurodegenerative diseases, can be conveniently manipulated in *Drosophila* via genetic mutation to give insight into processes in the neuron. Transport activity can be clearly imaged via dissection of larva and fluorescence microscopy of the dissected specimen.

**Materials and Methods:** *Drosophila* are cultured in 6 oz. polypropylene fly bottles. A mixture of water, molasses, cornmeal, yeast, agar, propionic acid, and tegosept is prepared as fly food and deposited into these bottles to fill their bottoms. The bottles containing flies are kept in rooms at typically 60% humidity and 18°C or 25°C depending on if a slower or more rapid growth rate respectively is needed. Fresh flies are allowed to mate and lay eggs for about 3 days, at which point the adult parents are discarded. Following eclosion of pupated larvae (about 9 days after fertilization), the adult flies are flipped into a new bottle with new food to breed and produce the next generation of flies, or sorted by sex for the purpose of crossing with another stock. In the manipulation of axonal transport, UAS lines are bred with stocks that express Gal4 in the nervous system in order to drive needed mutations. These UAS lines fluorescently tag vesicles and proteins of interest in selected neurons as well as generate mutations to be observed. Dissection is performed on 3rd instar larvae that are first placed on a culture glass containing calcium-free HL3 medium. The specimen is pinned and dissected on a sylgard gel. An epifluorescence wide-field microscope with a Photometrics CoolSNAP $HQ^2$ camera is used to perform live imaging of the specimens. The imaging software used is Nikon Elements (Version 4.0).

**Results and Discussion:** Following the dissection of a 3rd instar larva, the specimen is placed under an epifluorscence wide-field microscope. Tagged proteins and/or vesicles of interest fluoresce and are tracked over a defined period of time. Their movement is plotted in diagrams called kymographs (Figure 1). Patterns in velocity are mathematically analyzed using programs in MATLAB and R. These patterns offer insight into the processes of axonal transport that lead to neurological diseases when abnormal.

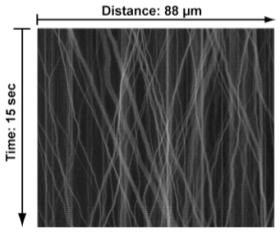


**Figure 1. Movement of an individual vesicle along an axonal segment represented by a plot of distance over time**

**Conclusions:** In the study of neurodegenerative diseases, *Drosophila melanogaster* provides a low-cost, simple, and well-characterized system in which to model neurological processes such as axonal transport. For instance, through genetic manipulation of the fruit fly, expression of Tau protein, a microtubule-associated protein associated with Alzheimer's Disease, can be altered and the effects of these mutations tracked through the methods presented here. While the procedure presented here provides good data, a protocol in which imaging does not require the dissection of the specimen may simplify the process as well as give better results. In conjunction with live imaging, fixing and immunostaining dissected subjects can give more insight into axonal transport as well. While *Drosophila melanogaster* is a great model organism, it is not mammalian and studies using mammalian specimens such as mice will have physiologically more relevant implications for human disease and physiology.

**Modeling the Role of Filopodia Energetics in Cell Morphology Dynamics**

Robert Morhard, Dr. Chris Bettinger - Department of Biomedical Engineering, Carnegie Mellon University

**Introduction:** Nanotopographic cues influence a variety of responses in mammalian cells. These cues can be important for stem cell differentiation, cell polarization and cell morphology. Current work in the Bettinger lab incorporates elastomeric polymers coated with a thin metallic layer while under strain. When this strain is released, the metallic layer buckles creating nano-grooves (Figure 1). Cells elongate along these nano-grooves, but the mechanism for this process isn't well understood. Recent evidence suggests that cell morphology changes are the result of decentralized, filopodia-membrane interactions. The cellular membrane surface tension and bending modulus determine the resisting force to actin-driven filopodia projections. In addition, filopodia that are aligned to the nano-grooves have higher density actin-rich networks due to strong focal adhesions. These focal adhesions resist the restoring membrane-based force and make filopodia parallel to the grooves more stable than filopodia perpendicular to the grooves. This study seeks to provide an energetic, decentralized model to explain cell morphology changes in response to nanotopography changes. This information will be useful in studying and predicting the behavior of neurons involved in peripheral nerve regeneration, among other fields.

**Materials and Methods:** Modeling was conducted on MATLAB and analysis was conducted on Microsoft Excel.

**Results and Discussion**: As filopodia length increases, the energy involved in resisting the membrane-based restoring force increases. This distance is a function of distance from the bulk cell membrane and the height of the substrate at that particular location. In addition to these energetics, individual projects are also more stable as they become more parallel to the nanogrooves. As stability decreases, the jumping frequency of each filopodia increases. Therefore, filopodia will have the lowest jumping frequency and the longest staying time when they are aligned parallel to the nanogrooves, at the top of a groove and not extending far from the bulk cell membrane. Thus far the model creates several relevant substrates, and plots the trajectory of filopodia dynamics on a substrate (Figure 2). It also stores the average staying time for each location to provide complete information.

**Conclusions:** The current model illustrates thermodynamically-realistic filopodia dynamics. Future work will incorporate this into a total cell model and plot cell ellipticity over time for each substrate. These results will confirm whether this decentralized mechanism is a feasible proposal for cell morphology changes.

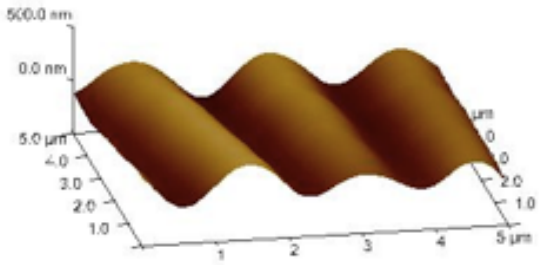


Figure 1: AFM image illustrating the nanogrooves of the substrate.

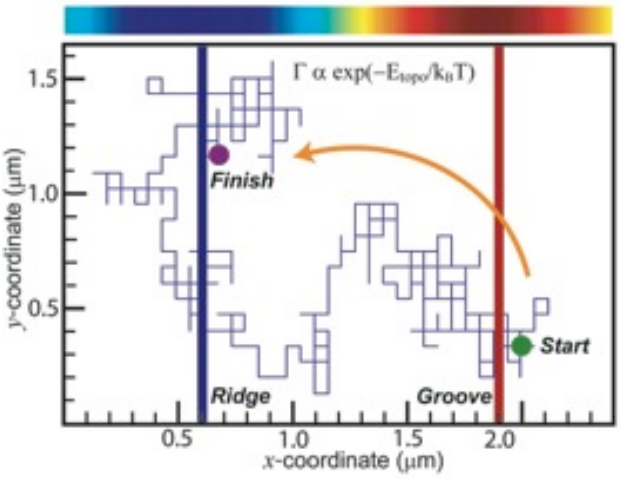


Figure 2: Filopodia trajectory with jump frequency formula and ridge and groove defined.

**ANALYSIS OF PRESERVON-TREATED RABBIT BONE TISSUE**

Dennis Shih, Amy Donovan. Bone Tissue Engineering Center

**Introduction:** There are several methods that allow proper preservation and processing of bone grafts, with the two most popular being Freezing and Freeze-Drying. In this study, research is focused on a new method of bone preservation – Preservon® - a proprietary, glycerol-based preservation solution created and used by LifeNet Health. The investigation places emphasis on comparing various aspects of bone growth among implants treated via freezing, freeze-Drying, and the Preservon® method.

**Materials and Methods:** *Ex Vivo:* Femurs were harvested from New Zealand White (NZW) rabbits and sent to LifeNet Health to be processed into cylindrical allografts (5mm diameter, 5mm length). The allografts were preserved via Preservon®-treatment, freeze drying, or freezing. In the lab, implants from each treatment group were processed using hard tissue histology techniques and ground sectioning to produce slides that were stained and photomicrographed at various magnifications using a light microscope. Scanning electron microscope (SEM) micrographs of implants from each group, as well as non-treated bone graft standards, were also analyzed.
*In Vivo:* A pilot animal study was done to observe morphological differences among bone allografts treated by the three different methods. Allografts were Preservon®-treated, freeze dried, or frozen (6 per treatment group). Nine skeletally mature female NZW rabbits received bilateral femoral plug implants in the medial condyle of the femur. Animal surgeries took place at the Allegheny-Singer Research Institute, following protocol approved by the Institutional Animal Care and Use Committee. Four weeks after implantation, the allografts and surrounding tissue were retrieved and underwent hard tissue histology. The specimens were dehydrated, xylene infiltrated, and embedded in poly(methyl methacrylate) (PMMA). The surrounding PMMA was reduced, and specimens were bisected and ground to ~30μm on a precision microgrinder. Once slides were produced, they were acid etched and stained with Goldner's Modified Trichrome stain. Photomicrographs of each specimen were taken at 1.25, 2.5, 5.0, 10.0, and 20.0x magnifications, focusing on the allograft-host interface. Each implant was then given a score from 0 to 3 for several biocompatibility characteristics: cortical integration, new cancellous bone growth, osteophilicity, osteoconduction, periosteal growth, medullary growth, and fibrosis, for a total of 18 points.

**Results and Discussion:** *Ex Vivo:* SEM micrographs revealed topographical differences among the three treatment groups. Freeze-dried and frozen implant surfaces showed dark and light regions, while the Preservon-treated samples were covered in a layer of deposit. Photomicrographs of histological specimens displayed the cortical and trabecular bone regions and emphasized the porosity of each implant.
*In Vivo:* Distinct traits of bone growth were observed in the histology processed slides. Freeze dried implants received an average biocompatibility of 14.3, frozen implants scored an average of 11.1, and Preservon-treated implants had an average score of 10.7. The freeze-dried implants showed excellent new cancellous bone growth, osteophilicity, and medullary growth. Frozen implants had varied scores across all categories, but displayed consistent levels of cancellous bone growth. Preservon-treatment resulted in the most fibrosis, but these implants had the greatest amount of periosteal growth.

**Conclusions:** This pilot study was able to demonstrate that allograft processing affects the integration of the graft into the host bone. Preservon®-treated allografts, while offering distinct advantages, were not the most biocompatible among the three groups. Collaboration with LifeNet Health on a more complete study with longer time periods and increased sample sizes, as well as histological processing methods that allow characterization of cellular mechanisms is anticipated.

**Acknowledgements:** The author would like to thank Amy Donovan, Dr. Jeffrey O. Hollinger, LifeNet Health, and the Carnegie Mellon Biomedical Engineering Department for their support and funding.

**Statistical and Mechanical Analyses on Needle Steering with Duty-Cycled Rotation**

Andre Sutanto, Craig A. Lehocky and Cameron N. Riviere. Carnegie Mellon University

**Introduction:** Traditionally, needle insertion into biological tissues can only be performed in straight paths. This method can prove to be problematic to reach locations deep within the human body, requiring longer needles and multiple insertions, which can increase risk of damage to the biological tissues and vasculature during the process. When inserted into tissue, flexible bevel-tipped needles naturally curve in the direction of the bevel due to tissue forces asymmetrically applied to the beveled surface. We have expanded upon this observation and developed a control scheme for navigating bevel-tipped needles along predetermined, non-linear paths by varying the orientation of the needle and alternating between spinning and not spinning the needle.This research ventures to improve the current system by performing statistical and mechanical analyses on various part of the needle steering project.

**Materials and Methods:** This project consisted of determination of artificial tissue parameters (A), a study of the effect of bevel angle on needle curvature (B), and a quantification of tissue forces exerted on needles during insertion with duty-cycled rotation (C):

A. Two artificial tissue simulants were prepared from Knox Gelatine at different consistencies. A ball-indentation procedure was implemented to determine the Young's modulus *(E)* of the tissue: A load-cell indenting tissue at 4 mm *(h)* for 15 minutes continuously recorded force data through LabVIEW. Eq. 1 was used to calculate Young's modulus (Henderson, 1985).

$$E = \frac{3(1-\upsilon^2)F}{4\sqrt{Rh^3}} \quad (1)$$

where $\nu$ is the Poisson Ratio, $F$ is the force applied and $R$ is the radius of the ball (3.175 mm for this project).

B. To quantify the effect of bevel angle on needle curvature, ten separate needles (four nitinol, three piano wire and three stainless steel needles) were rotary-filed to produce $20^o$ bevel tips, which were verified through light microscopy. Each needles was inserted into the tissue simulants at four rates of duty-cycled rotation: 0% (no spinning), 33%, 67% and 100% (constant spinning). Upon completion of needle insertion, the curvature of the needle path was quantified in MATLAB by fitting a circle to the needle arc. To show that the accuracy of the circle fit, a method, adapted from linear regression $R^2$ value calculation by floating both x and y values of each point in the arc, was written to quantify how good the circle fit was to any given needle path. [source]. This analysis was also applied to data previously collected on needles with $10^o$ beveled-tips.

C. To further analyze the needle insertion process mechanically; a modified system was assembled to measure the friction force experienced by the needle throughout the insertion process. The modification included designing and machining new aluminum parts and writing new LabVIEW interface to record the force of insertion during the needle insertion with duty-cycled rotation.

**Results and Discussion:** The ball indentation method yielded stiffness values of 35 kPa for Gel 1 and 48 kPa for Gel 2. When inserted into the tissue simulants, the $20^o$ needles exhibited needle curvature linear with duty-cycled rotation. Needle curvature increased with increasing tissue stiffness, decreasing needle radius, decreasing needle flexural rigidity, and decreasing bevel angle. These relationships were incorporated into a mechanical model encapsulating needle and tissue parameters to allow prediction of needle curvature based on duty-cycled spinning. Statistical analyses on goodness of fit for needle curvature quantified through circle fitting algorithms were performed on the experimental results gathered from ten different needles with bevel angles of $10^o$ and four different gels, as well as the $20^o$ needle results. The y-coordinates of the needle arcs adhered almost perfectly with the y-coordinates of the circle fit. Therefore, analyses were run by fixing the y-coordinates and calculating how well the x-coordinates of the needle path fit the x-coordinates of the circle, yielding an average $R^2$ value of 0.99 ($\pm$ 0.03).

**Conclusions:** Based on these experiments, it was established that the circle fitting procedure used in the project yielded very accurate results. Further experiments on ball indentation process; needle steering with various bevel angles and force measurement during the insertion process should be conducted to better understand the project.

**Human Motion Reconstruction from Body Mounted Accelerometer Data**

Gillian Tay, Mark Friedman. Carnegie Mellon University.

**Introduction:** The use of accelerometers has been increasing at a rapid rate due to the old age of this technology. Because of its size and cost, it is feasible to mount an array of accelerometers onto a subject for an extended period of time. This feature has applications in the field of medicine, specifically in physiotherapy. In the past it was impossible to monitor the activities of a physiotherapy patient beyond the time allotted for his or her appointment. Now, due to the increased availability of accelerometers, it has now become a possibility to use this acceleration data to reconstruct human motion in a way that a physical therapist, or an untrained accelerometer reader, may be able to easily comprehend.

**Materials and Methods:** The materials used included an array of accelerometers, a computer, and a software package. An array of accelerometers was mounted onto a subject to record acceleration data over a period of 24 hours onto 5 specific, predetermined locations on the body. This acceleration data was later downloaded from the accelerometers onto a computer. At this point, a software package was designed specifically for the sake of parsing this raw data into a graphical form. The parsing of the raw data includes calculating the magnitude and the direction of this acceleration. By parsing the raw data into a magnitudes and directions, it became feasible to reconstruct angles which could be translated to orientations of body parts. These orientations were then translated to a graphical display where lines would represent the body parts. When these graphical displays are shown in quick succession, the motions that the accelerometers had previously recorded could be reproduced as a "stick figure" version of the human motion.

**Results and Discussion:** By translating the motion of the accelerometers as human motion, graphical representations of human motion was constructed and developed into a runnable program. The "stick figure" was drawn by specifying start and end points of each limb of a predetermined length, based on a calculation of the angle from each accelerometer monitor. The angles were initially calculated using a one-dimensional tilt axis, focusing on the x-axis values, and then improved to a two-dimensional axis calculation, which decreased instances of noise and included a bigger range of movement drawn. An even better improvement was calculations based on a three-dimensional axis. However, there was a tradeoff between the target audience that the software package was being designed for - physiotherapists in elderly homes – who would have trouble understanding the values and calculations of a three-dimensional tilt axis, and so simplicity and comprehension was chosen over accuracy and functionality. As the accelerometer is now a relatively old technology, another trade-off of it being cost efficient, was the noise and inaccuracies that could be recorded, in random points, as well as in cases when the acceleration of the recorded motion exceeds gravity. Since the calculations are based on 1g (gravity), this was definitely a problem. To account for the noise, a running weighted average was created to try and minimize inaccurate representations.

**Conclusions:** A runnable software package was successfully designed to parse the raw data taken by the accelerometers, to a graphical format. However, due to not being able to account for every specific edge case for the two-dimensional axis angle calculations, the deployable package was compiled with one-dimensional calculations. This results in a workable program with a basic user interface to navigate through a 24+ hour data set, as well as an in-program timer with an automatic play-through feature.

**References:**

Clifford, Michelle. "Measuring Tilt with Low-g Accelerometers". Freescale Semiconductor: Application Note. 2005. AN3107.

Tuck, Kimberly. "Tilt Sensing Using Linear Accelerometers". Freescale Semiconductor: Application Note. 2005. AN3461.

**USING SURFACE INITIATED ASSEMBLY TO INVESTIGATE THE M ECHANICAL PROPERTIES OF FIBRONECTIN**

Rebecca Wells, John Szymanski, Martin Antensteiner, Adam W. Feinberg. Carnegie Mellon University.

**Introduction:** The extracellular matrix (ECM) is composed of protein fibers including fibronectin, laminin, fibrinogen, and collagen. It has been proposed that ECM proteins contain cryptic binding domains that become exposed in a force-induced manner. We are specifically focused on fibronectin (FN) because it is a major component of the ECM during wound healing and embryonic development, suggesting FN plays a key role in regenerative processes. Here, we used a technique termed surface-initiated assembly to suspend FN fibers across microfabricated trenches made out of polydimethylsiloxane (PDMS). These suspended fibers were then stretched with a micromanipulator to strains of ~ 150%.

**Materials and Methods:**

Photolithography: In order to perform this experiment, PDMS stamps for microcontact printing and release were first fabricated using photolithography. This involves spincoating photoresist onto a piece of glass which is then heated and exposed to UV light with a specifically patterned photomask on top of it. It is heated again and then the excess photoresist is removed by developing. This glass is then placed in a petri dish and coated with PDMS. Once the PDMS cures in the oven, the stamps can be cut out of the PDMS and removed from the glass.

Microcontact Printing: Stamps fabricated with photolithography are then used for microcontact printing. In this process, the PDMS stamps are first coated with fibronectin, of which 20 percent is labeled with Alexa Fluor 546 Malemide. Glass coverslips are then spincoated with poly(N-isopropylacrylamide) (PIPAAm). The PDMS stamp is placed on the PIPAAm coated coverslip and then removed.

FN Suspension: To suspend the fibers across the trenches, a heated stage consisting of a metal plate with an opening to hold a petri dish is used. Since PIPAAm will dissolve at 32 degrees Celsius, leaving just the FN fibers, this heated stage allows the temperature to remain constant prior to release. The PDMS trench stamp is placed in a petri dish in the heated stage, and a FN printed coverslip is placed on top such that the PIPAAm coated side is in contact with the trenches. Water at a temperature above 40 degrees Celsius is added and allowed to diffuse into the trenches. Once diffusion is complete, the heated stage is turned off and the temperature decreases until it reaches 32 degrees, where the PIPAAm will release. The glass coverslip is then removed, and the FN fibers should have suspended across the trenches.

FN Straining: To stretch these fibers, a micromanipulator is used with a capillary tube that has been extruded at the tip so it will fit in the trenches. The tip is then used to strain the fiber to its breaking point, and images are taken and then later analyzed to determine the stretched length.

**Results and Discussion:** While attempting to release the FN across the PDMS trenches, we determined that the ratio of trench depth to trench width must be approximately .5 in order for the fibers to suspend. During initial experimentation, two depths of trench were used, 20 μm and 40 μm. With the 20 μm deep trenches, widths of 50 μm, 100 μm, and 200 μm were used, and in all of these cases, the FN fibers followed the contour of the trenches rather than suspending across them. When 40 μm deep trenches were used, fibers suspended across 50 μm wide trenches, but followed the contour of the 100 μm and 200 μm wide trenches. Therefore, the ratio is between .4 and .8. Using a capillary tube that has been extruded to a fine tip, we were able to strain suspended fibers to strains of about 150%.

**Conclusions:** We have developed a reliable method to suspend FN fibers, so FN strain tests can now be performed easily. In the future, we plan to strain FN fibers and measure changes in binding activity, an indication of cryptic binding sites becoming exposed. We also plan to repeat this process with other ECM proteins, including laminin, collagen, and fibrinogen.